



Full length article

## Protein interactions with layers of TiO<sub>2</sub> nanotube and nanopore arrays: Morphology and surface charge influence



Mukta Kulkarni<sup>a,b,1</sup>, Anca Mazare<sup>b,1</sup>, Jung Park<sup>c,1</sup>, Ekaterina Gongadze<sup>a</sup>, Manuela Sonja Killian<sup>b</sup>, Slavko Kralj<sup>d</sup>, Klaus von der Mark<sup>e</sup>, Aleš Igljč<sup>a</sup>, Patrik Schmuki<sup>b,\*</sup>

<sup>a</sup>Laboratory of Biophysics, Faculty of Electrical Engineering, University of Ljubljana, Ljubljana, Slovenia

<sup>b</sup>Department of Materials Science and Engineering, WW4-LKO, University of Erlangen Nuremberg, Erlangen, Germany

<sup>c</sup>Division of Molecular Pediatrics, Department of Pediatrics, University of Erlangen-Nuremberg, Erlangen, Germany

<sup>d</sup>Department for Materials Synthesis, Jožef Stefan Institute, Ljubljana, Slovenia

<sup>e</sup>Department of Experimental Medicine I, Nikolaus-Fiebiger Center of Molecular Medicine, University of Erlangen-Nuremberg, Erlangen, Germany

### ARTICLE INFO

#### Article history:

Received 7 June 2016

Received in revised form 9 August 2016

Accepted 26 August 2016

Available online 28 August 2016

#### Keywords:

TiO<sub>2</sub> nanotube/nanopore

ELISA

Distribution of protein binding

Albumin

Histone

### ABSTRACT

In the present work we investigate the key factors involved in the interaction of small-sized charged proteins with TiO<sub>2</sub> nanostructures, i.e. albumin (negatively charged), histone (positively charged). We examine anodic nanotubes with specific morphology (simultaneous control over diameter and length, e.g. diameter – 15, 50 or 100 nm, length – 250 nm up to 10 μm) and nanopores. The nanostructures surface area has a direct influence on the amount of bound protein, nonetheless the protein physical properties as electric charge and size (in relation to nanotopography and biomaterial's electric charge) are crucial too. The highest quantity of adsorbed protein is registered for histone, for 100 nm diameter nanotubes (10 μm length) while higher values are registered for 15 nm diameter nanotubes when normalizing protein adsorption to nanostructures' surface unit area (evaluated from dye desorption measurements) – consistent with theoretical considerations. The proteins presence on the nanostructures is evaluated by XPS and ToF-SIMS; additionally, we qualitatively assess their presence along the nanostructures length by ToF-SIMS depth profiles, with decreasing concentration towards the bottom.

### Statement of Significance

Surface nanostructuring of titanium biomedical devices with TiO<sub>2</sub> nanotubes was shown to significantly influence the adhesion, proliferation and differentiation of mesenchymal stem cells (and other cells too). A high level of control over the nanoscale topography and over the surface area of such 1D nanostructures enables a direct influence on protein adhesion. Herein, we investigate and show how the nanostructure morphology (nanotube diameter and length) influences the interactions with small-sized charged proteins, using as model proteins bovine serum albumin (negatively charged) and histone (positively charged). We show that the protein charge strongly influences their adhesion to the TiO<sub>2</sub> nanostructures. Protein adhesion is quantified by ELISA measurements and determination of the nanostructures' total surface area. We use a quantitative surface charge model to describe charge interactions and obtain an increased magnitude of the surface charge density at the top edges of the nanotubes. In addition, we track the proteins presence on and inside the nanostructures. We believe that these aspects are crucial for applications where the incorporation of active molecules such as proteins, drugs, growth factors, etc., into nanotubes is desired.

© 2016 Acta Materialia Inc. Published by Elsevier Ltd. All rights reserved.

### 1. Introduction

Titanium (Ti) and its alloys are ideal implant biomaterials, due to their favorable biocompatibility and corrosion resistance [1]. Additionally, their surface properties influence the biological response and therefore nanoscale surface modifications have been extensively evaluated [2,3].

\* Corresponding author.

E-mail address: [schmuki@ww.uni-erlangen.de](mailto:schmuki@ww.uni-erlangen.de) (P. Schmuki).

<sup>1</sup> Authors contributed equally to the work.

TiO<sub>2</sub> nanostructures have found broad interest, as both nanotopography and high surface area significantly influence their use in biomedical applications (e.g. osseointegration, antibacterial activity, mitigate inflammatory response, etc.) [2,4–7]. Self-organizing electrochemical anodization is the preferred method for growing TiO<sub>2</sub> nanotubes (NTs) directly on Ti substrate, as it enables a good control over their geometry, long-range order and ease of application [8,9].

Recently it was shown that cells respond to the nanoscale dimensions of nanotubes, i.e. enhanced adhesion, proliferation and differentiation were observed on 15 nm diameter NTs [10,11], and can be synergistically influenced by NTs morphology and growth factors [12]. Other properties, e.g. charge distribution, materials size and chemistry, can also influence the adhesion of cells [13–15].

In a biological environment, proteins are always present at the material's surface as an intermediate layer further mediating cell attachment and proliferation [3,16] and as the first event occurring at the initial contact between implant's surface and biological environment (tissue, body fluids) is protein adhesion, their adsorption on Ti implants was widely investigated [17–20]. Briefly, it consists of the i) first (fast) adsorption, i.e. direct attachment of molecules arriving at the surface, and ii) second (slow) process – where rearrangement can take place, either by changes in molecular orientation, or by exchange with new arriving ones [17]. Other parameters, e.g. surface charge density or chemistry, topography, hydrophilicity, proteins isoelectric points, solution pH, further influence protein adsorption (for more information see Wilson et al. [20]).

From the above parameters, the electrical force occurring between proteins and surface of implant is crucial [9,15] and is generally evaluated by the isoelectric point (IEP), e.g. native Ti – IEP = 4.0 [21], fibrinogen – IEP = 5.5 [22], albumin – IEP = 5.0 [19], while for TiO<sub>2</sub> NTs values are in the 4.7–5.18 range (depending on NTs morphology) [23]. It was also reported that the difference in protein size contributes to their adsorption sites and thus to adhesion on Ti [19].

The above reviewed literature investigates compact TiO<sub>2</sub>, TiO<sub>2</sub> nanoparticles, nanorough Ti or other biomaterials. It is known that proteins adsorb more on TiO<sub>2</sub> NTs (compared to compact layers) due to their higher surface energy [24] and this leads to an increased initial protein adsorption. Thus enhanced cellular interactions occur as proteins mediate the interactions between the cell membrane and TiO<sub>2</sub>, both negatively charged [9,15,25,26]. Therefore, the principles elucidated from this work can offer guidance for the modification of the implant surface towards an optimised surface geometry and profile, to best fit the required protein and cell interactions.

Herein, we show the influence of the morphology of TiO<sub>2</sub> nanostructures (nanotubes – NTs and nanopores – NPs) on the adsorption of small-sized charged proteins. We obtain diameter-controlled and at the same time length-controlled anodic nanostructures for 15, 50 and 100 nm diameter series and we evaluate their interactions with small enough proteins (<10 nm) to enter all the investigated structures, as well as different charge i.e. albumin (negative) and histone (positive). The effect of protein characteristics to their adhesion leads to an adsorption trend based on the nanostructures' morphological characteristics, including also their surface charge density. Additionally, surface coverage of proteins is investigated by XPS and ToF-SIMS, whereas adhesion inside the nanostructures is followed with ToF-SIMS sputter depth profiles.

## 2. Experimental

### 2.1. Growth of anodic TiO<sub>2</sub> nanostructures

TiO<sub>2</sub> nanostructures are grown by electrochemical anodization of Ti foils (Advent, 0.1 mm thickness, 99.6% purity) that are cleaned by ultrasonication (acetone, ethanol and deionized water, for 5 min each) and dried in a N<sub>2</sub> stream. Anodizations are performed at room temperature (~22 °C) in a two-electrode cell (anode – Ti foil, cathode – Pt mesh, 15 mm working distance) using a two-step anodization approach – see Supplementary material (Fig. S1). The electrolytes used are ethylene glycol (EG) based (with specific water and hydrofluoric acid, 40%, content) – Table 1. After anodization, samples are kept in ethanol for 2 h, washed with distilled water and dried. Ultrasonication was performed only for NT<sub>100nm,7µm</sub> and NT<sub>100nm,10µm</sub>, to remove nanograss.

### 2.2. Surface and chemical characterization

The top and cross-section morphologies of TiO<sub>2</sub> arrays are observed using a field-emission scanning electron microscope (Hitachi FE-SEM S4800). Chemical composition is investigated by X-ray photoelectron spectroscopy (PHI 5600, spectrometer, USA) using AlK $\alpha$  monochromatized radiation (calibrated to Ti2p, 458 eV). Peak fitting is performed with Multipak software.

Time-of-flight secondary ion mass spectrometry (ToF-SIMS) surface spectra in positive and negative polarity are recorded on a ToF SIMS 5 instrument (ION-TOF, Münster, Germany). Negative depth profiles are recorded in dual beam mode, with a pulsed 25 keV Bi<sup>+</sup> liquid-metal ion beam (bunched down to <0.8 ns) for spectra generation and a 500 eV Cs<sup>+</sup> (15 nm diameter NTs/NPs) or a 2 keV Cs<sup>+</sup> ion beam (for 100 nm NTs) for sputter-removal, on a 50.8 × 50.8 µm<sup>2</sup> area in the center of 250 × 250 µm<sup>2</sup> sputter crater. Signals are identified according to their isotopic pattern as well

**Table 1**  
Anodization conditions (sample name shows diameter and length of nanostructures).

Sample name	Electrolyte	Potential used (V)	Anodization time
NP <sub>15nm,250nm</sub>	EG + 6 M water + 0.2 M HF	10 V	1 h
NT <sub>15nm,250nm</sub>	EG + 8 M water + 0.2 M HF	7 V	3.5 h
NT <sub>15nm,370nm</sub>	EG + 8 M water + 0.2 M HF	10 V	2.5 h
NT <sub>15nm,600nm</sub>	EG + 6 M water + 0.2 M HF	10 V	6 h
NT <sub>50nm,1µm</sub>	EG + 8 M water + 0.2 M HF	20 V	2.5 h
NT <sub>50nm,1.75µm</sub>	EG + 6 M water + 0.2 M HF	40 V	1 h
NT <sub>50nm,3.1µm</sub>	EG + 4 M water + 0.2 M HF	100 V	45 min
NT <sub>50nm,3.7µm</sub>	EG + 4 M water + 0.2 M HF	92 V	1 h
NT <sub>100nm,2.4µm</sub>	EG + 10 M water + 0.2 M HF	50 V	2 h
NT <sub>100nm,3.7µm</sub>	EG + 8 M water + 0.2 M HF	58 V	2.5 h
NT <sub>100nm,5µm</sub>	EG + 6 M water + 0.2 M HF	100 V	1 h
NT <sub>100nm,7µm</sub>	EG + 6 M water + 0.2 M HF	60 V	8 h
NT <sub>100nm,10µm</sub>	EG + 4 M water + 0.2 M HF	60 V	12 min
	+	+	+
	EG + 4 M water + 0.2 M HF	85 V	3 h

as exact mass. Spectra are calibrated to  $\text{CH}_2^-$ ,  $\text{C}_2^-$ ,  $\text{CN}^-$  and  $\text{CNO}^-$  (negative polarity) and  $\text{C}^+$ ,  $\text{CH}^+$ ,  $\text{CH}_2^+$ ,  $\text{CH}_3^+$  and  $\text{C}_7\text{H}_7^+$  (positive polarity) and Poisson correction is used.

Binding of 18 nm diameter colloidal gold-labelled goat antibodies (Jackson ImmunoResearch Laboratories, Inc., USA) to NTs structures is evaluated by dropping antibody solution (70  $\mu\text{l}$ ) on the samples (1  $\text{cm}^2$ ), incubating at 37 °C for 30 min, washing with distilled water (removal of unbound antibodies) and air drying. The gold-labelled antibody incubated NTs are mechanical scratched and characterized by transmission electron microscopy (TEM – JEM 2100, JEOL, Tokyo, Japan); the antibody solution is ten times diluted to facilitate easier TEM observation.

### 2.3. Protein adsorption and ELISA immunoassay measurements

Bovine serum albumin (albumin, Sigma Aldrich) and histone (H9250, Sigma Aldrich) proteins are used; 100  $\mu\text{l}$  of protein solutions (6 mg/ml) are applied on the  $\text{TiO}_2$  arrays samples (1  $\text{cm}^2$ ), incubated at 37 °C for 30 min and washed with 10 ml of phosphate buffered saline (PBS) solution under mild ultrasonication (37 Hz, 10% power, 60 s) to remove unbound protein. Finally, samples are air dried and used further for ELISA measurements. For XPS characterization of protein-coated samples, the above protocol is used and samples are dried in a spin-coater and immediately measured. To perform enzyme-linked immunosorbent assay (ELISA), a BCA protein assay kit (Thermo Fisher Scientific Pierce) is used and the standard procedure is followed (measurements are performed three times, in duplicate).

### 2.4. Evaluation of $\text{TiO}_2$ nanostructures surface area

#### 2.4.1. Dye desorption measurements

For dye sensitization, samples are immersed in 300 mM solution of Ru-based dye (cis-bis(isothiocyanato)-bis(2,2-bipyridyl)-4,4-dicarboxylato)ruthenium(II) bis-tetrabutylammonium), N719, in a mixture of acetonitrile and tert-butyl alcohol (1:1 v/v) for 1 day. Following, samples are rinsed with acetonitrile to remove non-chemisorbed dye. Dye desorption measurements of dye-sensitized samples are carried out by immersing samples in KOH (10 mM, 5 ml) for 30 min. The concentration of fully desorbed dye is measured spectroscopically (Lambda XLS UV/VIS spectrophotometer, Perkin-Elmer) at 520 nm and computed with Beer-Lambert law [27].

#### 2.4.2. Statistical computation of the top surface area of $\text{TiO}_2$ nanostructures

The total surface areas of NTs and NPs top surface are calculated per  $\text{cm}^2$  of sample, by using the  $A = \pi(R^2 - r^2)$  formula ( $A$  – surface area of the available top surface of the nanostructures;  $r$  – inner radius, half of the inner diameter of the NTs/NPs;  $R$  – outer radius, half of the outer diameter). Average values of inner/outer diameters are measured from SEM.

## 3. Results and discussion

In the following subsections, the main aspects are presented, that include the growth and optimization of  $\text{TiO}_2$  nanostructures (see Fig. 1), evaluating their influence on protein adhesion by ELISA measurements, surface electric potential modelling, establishing the key morphological parameters of  $\text{TiO}_2$  nanotubes influencing histone and albumin adhesion and a qualitative quantification of the proteins coating on the structures (on the top surface and in depth).

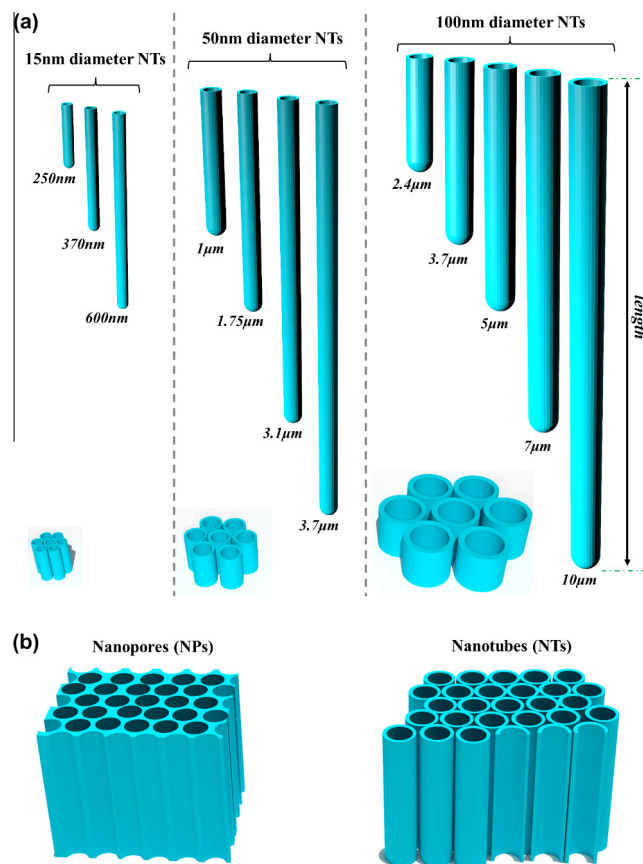


**Fig. 1.** a) Schematic overview of the different length NTs series used: 15, 50 and 100 nm diameter; b) Schematic representation of nanopores (NPs) and nanotubes (NTs).

### 3.1. Growth of $\text{TiO}_2$ nanotube and nanopore with specific diameters and lengths

The nanostructure morphology was specifically tailored to allow a simultaneous control over diameter and length. 15, 50 and 100 nm diameter NTs series were obtained, each with an increasing nanotube length (see overview in Fig. 1.a). In addition, for small diameters, different nanostructures can be grown (Fig. 1.b), i.e. nanopores (NPs) and nanotubes (NTs). NPs were previously reported in low-water content electrolytes [28], and as opposed to NTs possess a honeycomb structure with no tube to tube separation; the NP-NT transition occurs through a pore-wall-splitting mechanism [28,29]. The timeframe of this transition is controlled by the anodization parameters (water content, potential, time) [29] – it still occurs for increased water content, is time-dependent and accompanied by a slight diameter increase (Fig. 2.a).

SEM images of the different diameter NTs series are shown in Fig. 2.b–m. The anodization conditions are listed in Table 1 and were varied to ensure the desired morphology. E.g. to obtain longer NTs with similar diameter, we reduce the water content and additionally increase the potential: for  $\text{NT}_{100\text{nm}, 3.7\mu\text{m}}$  water content of 8 M and potential of 58 V, compared to 10 M, 50 V for  $\text{NT}_{100\text{nm}, 2.4\mu\text{m}}$ , etc. As high voltage anodization can lead to a thinning of NTs tops (i.e. a diameter increase), potential is decreased and time increased, to ensure similar top morphologies for same electrolytes (cf.  $\text{NT}_{50\text{nm}, 3.1\mu\text{m}}$  and  $\text{NT}_{50\text{nm}, 3.7\mu\text{m}}$  or  $\text{NT}_{100\text{nm}, 5\mu\text{m}}$  and  $\text{NT}_{100\text{nm}, 7\mu\text{m}}$ ). Only for  $\text{NT}_{100\text{nm}, 10\mu\text{m}}$ , a sacrificial protection layer is first grown (more details in Supplementary, Fig. S2).

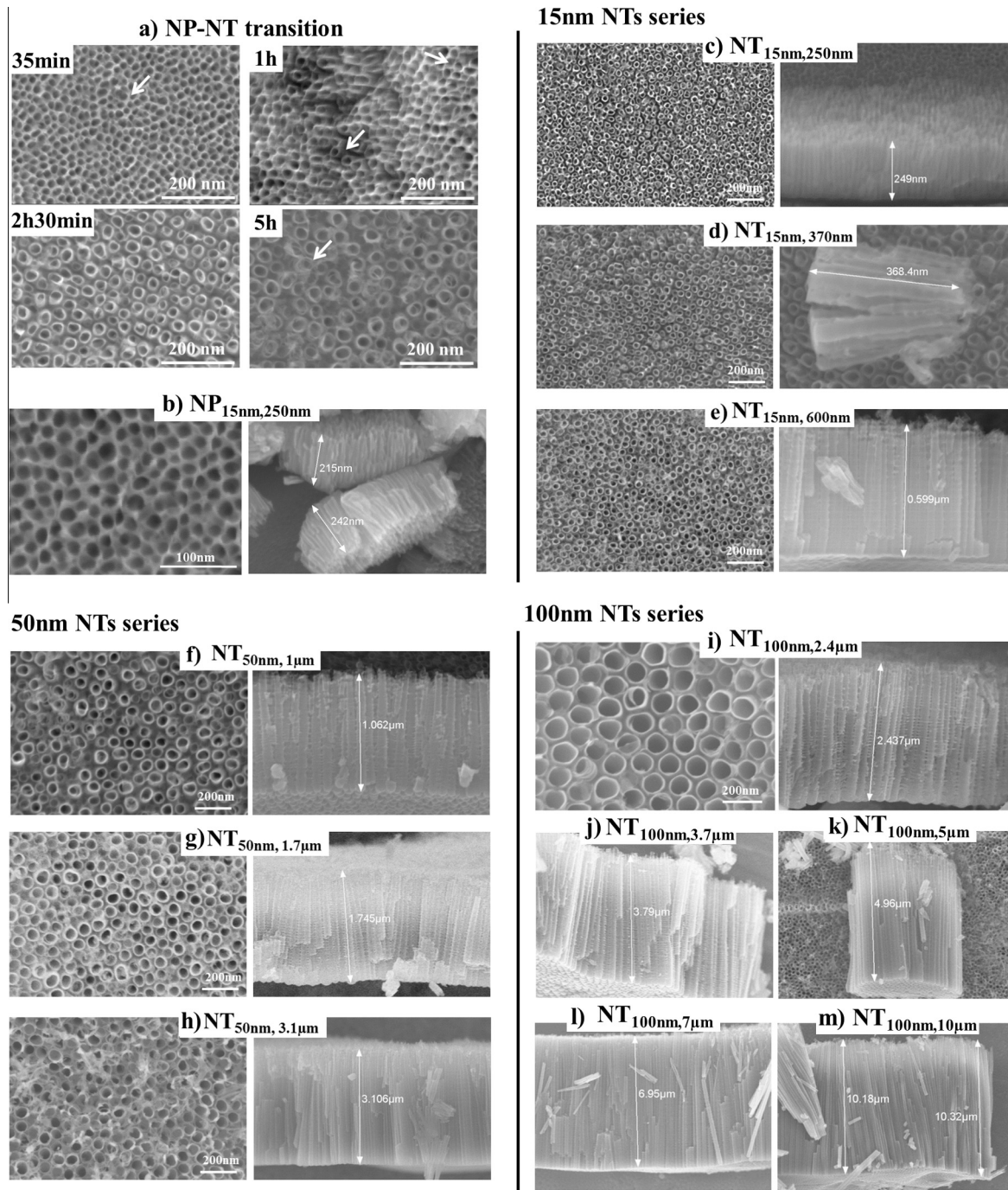


**Fig. 2.** a) NPs to NTs time-dependent transition (for  $NT_{15nm, 370nm}$ ); SEM images of: b) 15 nm NPs, c–e) 15 nm NTs series (250, 370 and 600 nm length); f–h) 50 nm NTs series (1, 1.7 and 3.1  $\mu m$ ); i–m) 100 nm NTs series (2.4–10  $\mu m$ ).

All NTs series present highly ordered, uniform and defect-free morphologies (Fig. 2) and these nanostructures ensure a length evaluation while keeping the diameter constant. 15 nm NTs show a 140% increase in length – from 250 to 670 nm, for 50 nm series, length varies from 1 to 3.7  $\mu m$ , whereas for 100 nm series from 2.4 to 10  $\mu m$ .

### 3.2. Protein adhesion on $TiO_2$ nanostructures as a function of nanostructure morphology

In the present study, to verify whether surface charge affects protein incorporation inside the nanotubes, we selected small size

globular proteins with opposite charge, i.e. histone – positive, bovine serum albumin – negative, instead of relatively large molecules proteins as fibronectin ( $\approx 120$  nm length, 2 nm thickness) [30,31].

For small size proteins, literature either report only one NTs morphology (e.g. albumin [24]) or for different diameters but not with different protein charge and control of NTs surface area (plasma proteins [26], albumin [32]). In this view, our work ensures both protein charge and surface area evaluation.

The reported size of the chosen proteins are  $\approx 7$  nm diameter (disk  $\approx 6.5$  nm in diameter) for the histone octamer [33,34], and  $\approx 8$  nm diameter with  $7.5 \times 6.5 \times 4.0$  nm [35,36] for albumin. The

protein size as a function of molecular weight, volume and shape is expressed by the Stokes radius ( $R_s$ ) i.e. experimentally determined effective hydrodynamic radius of a protein or radius of an equivalent sphere, including attached ions and water molecules [37]. An  $R_s$  of 3.55 nm [35] is reported for albumin, while for the histone octamer the hydrodynamic size is not known with certainty (the estimated  $R_s$  is 6.03 nm), however as only 70% of the protein is visible in the disk model [33], with extension/disordering of the polypeptide chain “tails” it increases to 6.8 nm and, if more predominant, to 7.9 nm (artificially stabilized octamer,  $R_s$  is 7.9 nm) [38]. Additionally, an  $R_s$  of 4.93 nm was measured when the octamer was exposed to physiological ionic strength media in absence of DNA (it dissociated in heterodimers and tetramers on a time scale faster than 1 s after mixing) [38].

Regarding the proteins' electric charge, the IEP of albumin is 5.0 [19], of histone is 10.23–11.36 (depending on its fraction) [26,39] and for  $\text{TiO}_2$  NTs is 4.7–5.17 [26]. Thus, at physiological pH,  $\text{TiO}_2$  arrays and albumin have a negative charge, while histone is positive. Additionally, all histone fractions are basic and have a net charge of +19 to +22 unit charges [26,39,40], whereas -13 unit charges is reported for albumin [41] (albumin's net charge, conformation and  $R_s$  are pH dependent [42–44], e.g. pH 6.8, -11 unit charges [42]; pH 8.0, -20 unit charges [43]; pH 10, -39 unit charges [42]).

### 3.2.1. Quantification of albumin and histone adsorption to $\text{TiO}_2$ nanostructures by ELISA

One of the most straightforward methods of evaluating the amount of protein bound to nanostructures is by ELISA immunoassay. All nanostructures listed in Table 1 were tested by ELISA and

measurements are shown in Fig. 3a – the highest quantities of adsorbed proteins are for 100 nm NTs, for the highest NTs length used in this study – 10  $\mu\text{m}$ . The charge of the used proteins is crucial as, at a physiological pH,  $\text{TiO}_2$  has a negative charge [26] and as such, from the negative albumin and positive histone, will attract more the positive protein; histone shows a twofold increase in adsorption onto all nanostructures. For NPs, the amount of albumin was below the detection limit, meaning that  $\text{NT}_{15\text{nm},250\text{nm}}$  ensure a better adhesion of albumin. In addition, for each diameter series, as expected, due to protein binding to the walls of NTs, the layer's length contributes to the quantity of adsorbed protein, irrespective of protein charge.

This raises the question if the increase in protein adhesion is only due to the higher surface area available; moreover, in literature ELISA measurements for small size proteins are not correlated with the NTs' surface area [26,45]. One can estimate the surface area by computation, however due to the morphology of NTs, i.e. “V-shape” of NTs (see Fig. S3, namely NT inner diameter is decreasing and wall thickness is increasing towards the bottom) and the spacing in between NTs (e.g.  $\text{NT}_{15\text{nm}}$ ,  $\text{NT}_{50\text{nm}}$  and  $\text{NT}_{100\text{nm}}$  average top spacing of  $6 \pm 2$  nm,  $21 \pm 4$  nm and  $30 \pm 5$  nm, respectively), it is exceedingly difficult to ensure an accurate computation. For this, we performed dye desorption measurements that allow a higher accuracy, due to the dye's penetration inside and in between NTs – the amount of dye adsorbed to nanostructures leads to a normalized surface area (see Table S1 and Fig. S4). A Ru-based dye was used, that is widely employed in dye sensitized solar cells for  $\text{TiO}_2$  nanotubes sensitization.

When the amount of adsorbed proteins is normalized with the dye desorption data (Table S1), it is clearly evident that overall

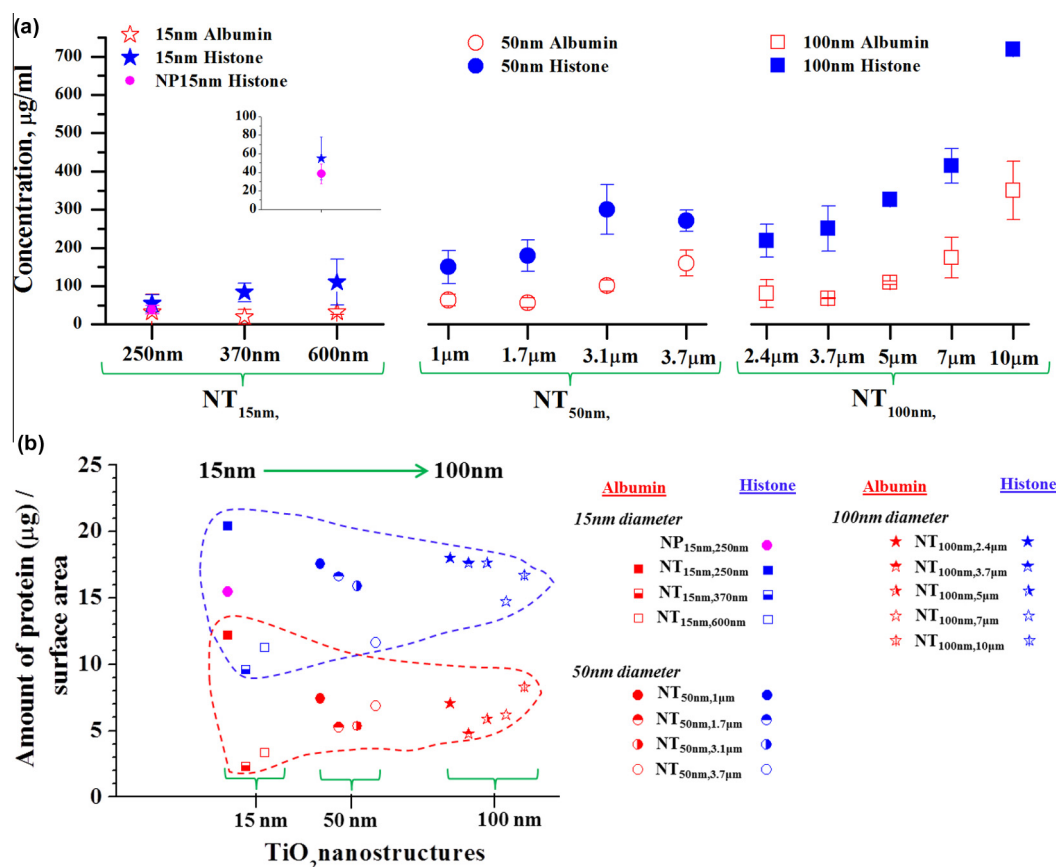


Fig. 3. a) Concentration of protein adhesion (albumin, histone) on  $\text{TiO}_2$  nanostructures as obtained from ELISA measurements; b) Amount of adsorbed protein normalized with the dye desorption values (Table S1, Fig. S4).

almost two times more histone is adsorbed (Fig. 3.b), due to the protein charge effect. With increasing length of NTs, there is a small decrease in the adsorbed histone (possibly due to wetting inside the NTs, i.e. penetration depth of solution inside and capillary filling effects on TiO<sub>2</sub> nanostructures [23,46,47]). For example, NT<sub>15nm,250nm</sub> adsorbs the highest amounts of normalized proteins with 12.1 µg albumin or 20.3 µg histone, while NT<sub>50nm,1µm</sub> adsorbs 7.5 µg albumin or 17.4 µg histone, and in 100 nm series there is NT<sub>100nm,2.4µm</sub> with 6.9 µg albumin or 18.0 µg histone, and NT<sub>100nm,10µm</sub> adsorbing more albumin (8.2 µg) but slightly less histone (16.7 µg) than NT<sub>100nm,2.4µm</sub>. For albumin, the protein amount going inside the NTs is further limited by its charge (repulsion with neighboring TiO<sub>2</sub> or with other bound albumin). Moreover, the NPs/NTs difference is evidenced, i.e. while dye desorption surface area measurements indicate only a 8.5% increase for NTs (from 2.34 nM, NP<sub>15nm,250nm</sub>, to 2.54 nM), histone adhesion increases with 31% (from 15.5 µg to 20.3 µg, normalized to dye desorption). Therefore, this increase cannot only be explained through the surface area of NTs, and can be due to surface charge effects.

### 3.2.2. Surface charge density distribution of TiO<sub>2</sub> nanotubes

Since albumin and histone bear net electric negative and positive charge, respectively, and nanostructured TiO<sub>2</sub> surfaces are also negatively charged [26], the difference in surface charge density between the inner/outer surface of NTs and inner surface of NPs can be estimated and correlated with the experimental results of Fig. 3.

The difference in surface charge density between the outer (convex) surface of the negatively charged TiO<sub>2</sub> nanotubes and the surface charge density of the inner (concave) surface of TiO<sub>2</sub> NTs/NPs, both in contact with an electrolyte solution, was estimated in this work using a simple electrostatic model of curved charged surfaces in contact with an electrolyte solution. The presented theoretical analysis is based on the specific morphological/geometrical details of highly curved TiO<sub>2</sub> NTs/NPs surfaces presented in this work. The specific physical properties of the TiO<sub>2</sub> surface are taken into account only through the value of the negative surface charge density of planar TiO<sub>2</sub> surface  $\sigma$  which is  $\approx -0.1 \text{ C m}^{-2}$ , as estimated from the Zeta potential measurements of flat TiO<sub>2</sub> surface at physiological conditions, given in [23].

The majority of theoretical models of an electrolyte solution in contact with a charged surface, including the classical Poisson-Boltzmann (PB) [48–50], assume that the relative (dielectric) permittivity ( $\epsilon_r$ ) is not space dependent but constant [51–53]. Therefore, classical PB theories have been upgraded by hydration models, where the interplay between solvent polarization and the diffuse double layer is taken into account [51–54]. In the current work, the electric surface potential and surface charge density at the inner (concave) and outer (convex) surface of the nanotube in contact with an electrolyte solution were calculated within the GI model [53] which takes into account the decrease of relative permittivity near the charge surface due to the orientational ordering of water dipoles, and the finite size of ions [53,55]. The model equations were solved numerically by using the Comsol Multiphysics 4.3a software program package (Stockholm, Sweden) and taking into account the appropriate boundary conditions [55], assuming that in thermodynamic equilibrium, the surface potential everywhere in the system is equal.

Fig. 4 presents the calculated surface charge density on the concave and convex tubular surfaces as a function of the magnitude of surface curvature radius ( $R$ ), i.e. the magnitude of the surface charge density on the outer convex nanotube surface is increasing, while on the inner concave NTs/NPs surface it is decreasing. Furthermore, the difference in surface charge density between the outer and inner NTs surface is not very high, even for radii  $\approx 7 \text{ nm}$  corresponding to 15 nm diameter NTs/NPs.

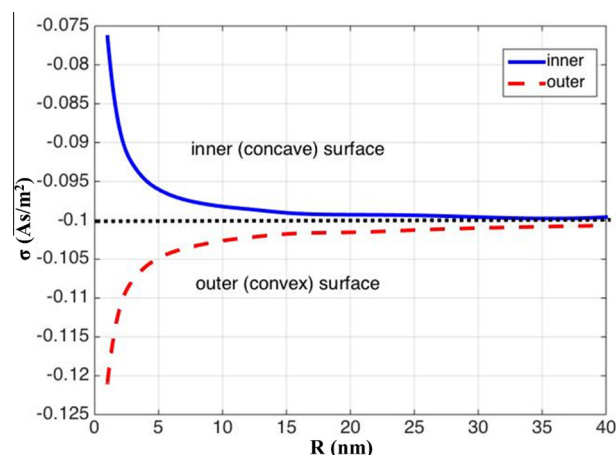


Fig. 4. Surface charge density on concave (blue line) and convex (red line) cylindrically curved surface as a function of curvature radius ( $R$ ) calculated for surface charge density of planar surface  $\sigma = -0.1 \text{ C m}^{-2}$ , temperature  $T = 298 \text{ K}$ , bulk concentration of ions  $n_0/N_A = 0.1 \text{ mol/l}$ , dipole moment of single water molecule  $p_0 = 3.1 \text{ D}$  and bulk concentration of water  $n_{0w}/N_A = 55 \text{ mol/l}$ . (For interpretation of the references to colour in this figure legend, the reader is referred to the web version of this article.)

On the other hand, the curvature radius of the NTs and NPs rims/edges at their top surface is very small (i.e., the curvature is very high). Therefore, in accordance with results presented in Fig. 4 and our previous theoretical consideration [9,15], the surface charge density of NTs/NPs wall edges at the NTs/NPs top surface is substantially increased, leading to increased electrostatic attraction of positively charged particles, increased electrostatic attraction of positive domains of particles with distinctive internal charge distribution and also to stronger mediated interaction between like-charged TiO<sub>2</sub> and cell surfaces [15,55]. This may explain why molecules (cells) are most strongly bound along the sharp convex edges or spikes of nanostructured Ti (where surface charge density and electric field strength are the highest) [55,56], and for the reported increased divalent cation-mediated fibronectin and quadrupolar protein-mediated adhesion of osteoblasts on low diameter TiO<sub>2</sub> NTs surfaces [9,15,31,55].

### 3.2.3. TiO<sub>2</sub> nanopore and nanotube interactions with proteins: surface charge and surface area dependence

Taking into consideration the normalized data for proteins adsorption on the different morphology nanostructures, the morphological characteristics of the used nanotubes and the surface charge density distribution, these data indicate that the difference in protein binding is therefore mainly determined by the difference in the surface area available for their binding, i.e. including the top surface of the NTs/NPs surface as well as the inner and outer surface of the NTs (for NPs only the inner surface). As there is no large difference in surface charge density between the inner NTs/NPs surface and outer NTs surface, albumin/histone can also bind to the inner and partially to the outer surface of NTs (if there is enough space, due to steric and charge restrictions).

The possibility of protein adhesion to the outer surface of NTs is due to the spacing at the top, in between NTs, that ensures additional adhesion area, and for NT<sub>50nm</sub> and NT<sub>100nm</sub> (spacings of  $\approx 21 \text{ nm}$  and  $\approx 30 \text{ nm}$ , respectively) both proteins are likely to enter. However, for NT<sub>15nm</sub> ( $\approx 6 \text{ nm}$  spacing), considering the proteins' hydrodynamic radius (albumin  $R_s = 3.55 \text{ nm}$ , histone  $R_s \approx 4.9 \text{ nm}$ ) both could fit, but histone is more likely to enter due to less charge induced effects with the neighboring negative TiO<sub>2</sub>.

The difference between NPs and NTs, NT<sub>15nm,250nm</sub> and NP<sub>15nm,250nm</sub>, is that NT<sub>15nm</sub> have highly curved rims at the top,

both on the inner and outer wall (0.39 cm<sup>2</sup> total available top surface area per cm<sup>2</sup> of sample), while NP<sub>15nm</sub> have at top surface only inner rims plus the TiO<sub>2</sub> surface connecting NPs (0.55 cm<sup>2</sup> total available top surface area).

At the highly curved rims there is, due to the small curvature radius, an increased magnitude of the surface charge density at the wall edge, i.e. at the nanotube top – as shown in Fig. S5a. NTs have ≈two time higher length of wall top edges per unit top area compared to NPs (Figs. 2, S5b) that may result in higher protein adhesion for both histone and albumin. Due to the high negative surface charge, the rims can promote the binding of positively charged proteins (also proteins with positively charged domains) or of proteins with internal charge distribution (possessing positively and negatively charged domains [9,15]).

The high local charge densities at the rims of the NTs or NPs top surfaces correspond to high electric field strength ( $E$ ) values of  $\sim 10^8$  V/m). In this strong electric field, the protein dipoles rotate to align in the direction of the electric field vector in order to minimize their potential energy. Consequently, proteins may undergo conformational changes [57] which can be then reflected also in alteration of the protein functions.

Albumin (negative) can bind to the negative TiO<sub>2</sub> NTs, although substantially weaker than histone, and this is possible due to the positively charged domains of albumin, as recently explained theoretically and also by Monte Carlo simulations in Refs. [10,17,55]. This and the NPs smaller amount of rims, explains why albumin binding to NP<sub>15nm</sub> is so weak. Namely, even if the positive domain of an albumin molecule is attached to the inner surface of NP<sub>15nm</sub> surface, its negatively charged domains protrude outwards from the surface and are close either to the opposite negatively charged TiO<sub>2</sub> surface or if another protein molecule fits in (if big enough diameter to allow it), to the negative domains of the albumin

bound to the opposite side of the surface. Both situations are not energetically favorable (steric hindrance). On the other hand, compared to NPs, the binding of albumin to the outer surface of NT<sub>15nm</sub> is theoretically possible. Similar occurrences can take place for NT<sub>50nm</sub> or NT<sub>100nm</sub>, due to the V-shape interior. To note that by normalizing the amount of adsorbed protein with the dye desorption measurements (dye size  $\approx 1$  nm), we account for both “V-shape” and spacing between NTs.

### 3.3. Qualitative assessment of protein location in TiO<sub>2</sub> nanostructures

#### 3.3.1. TEM investigations of gold-labelled antibodies on nanotubes

Currently, there is no existing literature on following the binding place of proteins inside nanostructures. It is well known that proteins adhere better on nanostructured surfaces (compared to flat), and this is observed in the NTs surface modification after immersion in cell culture media (SEM [58,59]) or by XPS [60]. Nevertheless, to follow the possibility of proteins binding in the NTs interior and/or in between NTs, we used diluted solutions of gold-labelled antibodies as protein substitutes to observe their binding ability using TEM analysis. The size of gold particles in the gold-labelled antibodies is of  $\approx 18$  nm, hence for 15 nm NTs they could only be observed on the top. As expected, gold-labelled antibodies were observed in the interior of 50 and 100 nm NTs (Fig. S6.a–c for NT<sub>50nm,1μm</sub> and d–f for NT<sub>100nm,3.7μm</sub>). Moreover, for the 100 nm NTs (Fig. S6.f), gold-labelled antibodies were also present in the spacings in between NTs.

#### 3.3.2. XPS characterization of protein coated TiO<sub>2</sub> nanostructures

To confirm the presence of proteins, XPS characterization was performed on selected samples (NP<sub>15nm,250nm</sub>, NT<sub>15nm,250nm</sub>, and NT<sub>100nm,7μm</sub>); Fig. 5 shows the high-resolution (HR) C1s and N1s

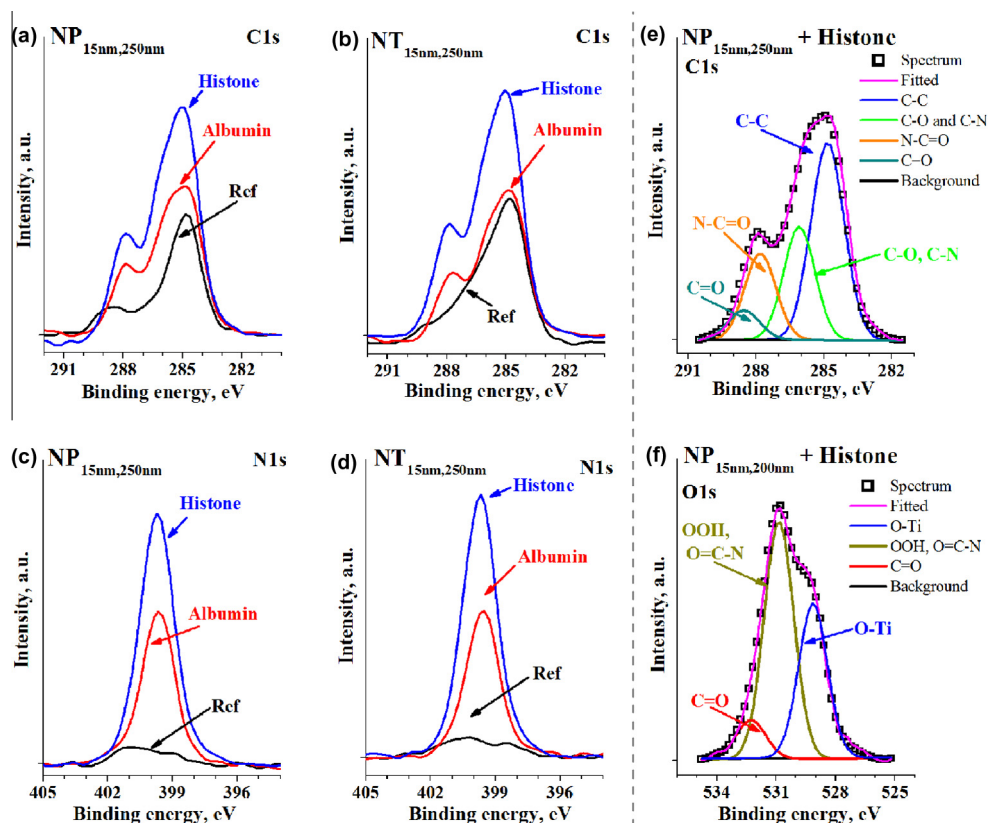


**Fig. 5.** XPS spectra of 15 nm NPs and NTs (as formed – Ref, albumin/histone coated): a–b) C1s, c–d) N1s, respectively. Peak deconvolution for histone NP<sub>15nm,250nm</sub>: e) C1s and f) O1s.

spectra for 15 nm NPs/NTs (O1s and Ti2p spectra are listed in Fig. S7). Significant differences are observed in the C, N and O peaks of protein coated samples (see also Table S2). The N content initially present in samples is very small and due to protein adsorption there is a significant increase, from 1 to 10 at.% and 16 at.% N for albumin and histone, respectively (the small amount of N in the reference sample, i.e. 1 at.% N, is due to pick-up from the environment). At the same time, we observe higher C amounts on protein coated samples, corresponding to hydrocarbons (C–C) at 284.8 eV, hydroxyl carbon (C–O) or nitrogen bound carbon (C–N) at  $\approx 286$  eV, amide carbon (N–C=O) at  $\approx 287.7$  eV and in carbonates (O=C–OH) at  $\approx 288.5$  eV [19,61,62] – see Fig. 5.e for an example of C1s peak fitting and Table S2 for the fitted results. Another significant difference is in the O1s peaks (see Figs. S7.a and 5.f), i.e. a decrease in the O peak attributed to  $\text{TiO}_2$  ( $\approx 529$ – $530$  eV) with an increase in the shoulder at  $\approx 531.7$  eV (binding energies of amide bonds overlaps with that of –OOH groups) [19].

100 nm NTs present similar trends, i.e., significant increases in C and N content (see Table S2), as well as the differences in the O1s peak. As XPS provides the composition in the first 3–10 nm of the surface and the N content is only due to the proteins, the N/Ti ratio (Table S2) indicates more albumin on top of 15 nm NPs (as compared to NTs), while for histone the 100 nm NTs show the highest ratio. Also, in 2D representation, there is a decreasing ratio of  $\text{TiO}_2$  top surface areas, i.e. 15 nm NPs > 15 nm NTs > 100 nm NTs (1:0.71:0.56 area ratio, respectively).

### 3.3.3. ToF-SIMS characterization of the protein coating on $\text{TiO}_2$ nanostructures

ToF-SIMS surface spectra in positive and negative polarity were recorded for the protein coated nanostructures (though complete

molecular fragments of proteins cannot be detected, low  $m/z$  characteristic fragments caused by amino acids can); an example for 15 nm NTs (reference, with albumin or histone) is shown in Fig. S8, revealing for positive polarity, a decrease of  $\text{Ti}^+$  ( $m/z$  47.90) and  $\text{TiO}^+$  ( $m/z$  63.90) fragments and increase of a variety of signals characteristic for amino acids, e.g., Arg –  $\text{CH}_3\text{N}_2^+$  ( $m/z$  43.03), Ser –  $\text{C}_2\text{H}_6\text{NO}^+$  ( $m/z$  60.03) etc. [63–66]. In negative polarity, clear signals of the peptide backbone are observed ( $\text{CN}^-$   $m/z$  26.00,  $\text{CNO}^-$   $m/z$  46.00) [67] and of PBS remnants ( $\text{PO}_2^-$   $m/z$  62.97;  $\text{PO}_3^-$   $m/z$  78.96) [67].

Fig. 6.a shows a comparison of the sum of amino acid fragments (positive polarity, please refer to Table S3 for a complete list of the signals used) and  $\text{Ti}^+$ , for the selected samples  $\text{NP}_{15\text{nm},250\text{nm}}$ ,  $\text{NT}_{15\text{nm},250\text{nm}}$ ,  $\text{NT}_{100\text{nm},3.7\mu\text{m}}$  and  $\text{NT}_{100\text{nm},7\mu\text{m}}$ . The observed trends are in agreement with the ELISA measurements (Fig. 3). Histone coated samples show significantly higher ratios compared to albumin; thus histone adsorbs better to the tube tops than albumin, within the ToF-SIMS information depth ( $\sim 1$ – $3$  nm). For albumin, 15 nm arrays show a higher protein/ $\text{Ti}^+$  ratio compared to 100 nm; while for histone higher ratios are for 100 nm NTs (this increase can be due to a decrease in  $\text{Ti}^+$  signal, in agreement with XPS data).

To investigate the proteins distribution inside the nanostructures, sputter depth profiles were performed for  $\text{NP}_{15\text{nm},250\text{nm}}$  (Fig. 6.b),  $\text{NT}_{15\text{nm},250\text{nm}}$  (Fig. 6.c) and  $\text{NT}_{100\text{nm},7\mu\text{m}}$  (Fig. 6.d); the main signals that can be easily followed are from the peptide backbone of proteins, i.e.  $\text{CN}^-$  and  $\text{CNO}^-$ . For clarity, we present the depth profiles for histone coated and reference sample and we show only the  $\text{Ti}^-$  (indicative of reaching the oxide/metal interface),  $\text{TiO}_2^-$  and  $\text{CNO}^-$  signals. The sharp decrease in signals observed for some depth profiles in the beginning, is due to the

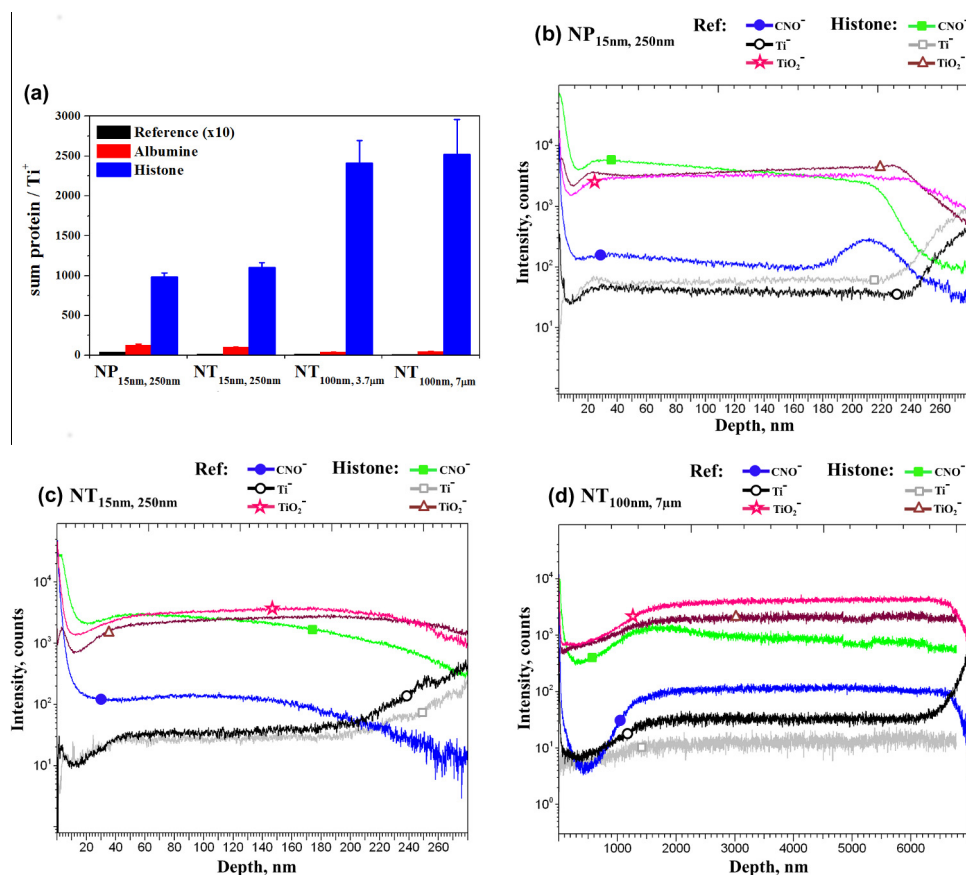
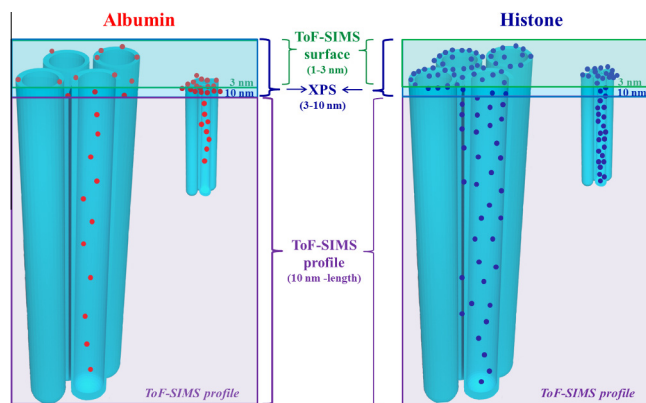


Fig. 6. a) Sum protein signals/ $\text{Ti}^+$  ratios from ToF-SIMS positive surface profiles for selected samples:  $\text{NP}_{15\text{nm},250\text{nm}}$ ,  $\text{NT}_{15\text{nm},250\text{nm}}$ ,  $\text{NT}_{100\text{nm},3.7\mu\text{m}}$  and  $\text{NT}_{100\text{nm},7\mu\text{m}}$  (Reference 10-fold increased). Negative ToF-SIMS sputter depth profiles for reference (Ref) nanostructures and with histone: b)  $\text{NP}_{15\text{nm},250\text{nm}}$ , c)  $\text{NT}_{15\text{nm},250\text{nm}}$ , d)  $\text{NT}_{100\text{nm},7\mu\text{m}}$ .



**Fig. 7.** Schematic overview of protein distribution obtained from ToF-SIMS top data (1–3 nm depth), XPS (3–10 nm depth) and ToF-SIMS sputter depth profiles (from a depth of 10 nm to the whole length). ELISA measurements account for proteins on the top and inside NTs.

time needed for  $\text{Cs}^+$  incorporated from the sputter beam to equilibrate [68]. Throughout the length,  $\text{CNO}^-$  signals are at least one order of magnitude higher for histone coated vs. reference samples and decrease towards the interface (where  $\text{Ti}^-$  increases and  $\text{TiO}_2^-$  decreases, these signals are comparable).

The proteins are present over the whole length of NTs, with slightly decreasing concentration towards the interface; generally,  $\text{CNO}^-$  signal for albumin is lower than for histone, see Fig. S9 (profiles for 15 nm NTs: histone, albumin, reference samples). An exception was  $\text{NP}_{15\text{nm},250\text{nm}}$ , where no peptide backbone signals were detected for albumin compared to reference (data not shown), correlating nicely with the ELISA data, where albumin was below detection limit.

ToF-SIMS sputter depth profiles of organic coated NTs represent a feasible method of qualitatively checking the coating inside the arrays.

To summarize, the results from ELISA measurements (Fig. 3), surface charge density modelling (Fig. 4 and S5), XPS (Fig. 5) and ToF-SIMS (Fig. 6, surface and sputter depth profiles), can be schematically represented in Fig. 7. Top surface evaluation data, i.e. XPS (3–10 nm) and ToF-SIMS (1–3 nm surface resolution), indicate higher amount of histone than albumin on all nanostructures. Additionally, a higher amount of albumin is bound to the 15 nm NTs. Sputter-depth profiles do not include the top surface (as at least 10 nm are needed to reach Cs-implantation equilibrium [68]), however they confirm the presence of the protein in the length of the nanostructure. Moreover, the reliability of using the  $\text{CNO}^-$  signal to track the peptide bonds of the protein inside the nanostructures is proven by the fact that for NPs there was no albumin detected in depth, correlating with XPS and ELISA data.

#### 4. Conclusion

We show the importance of the nanostructure topography and the necessity of a good control over  $\text{TiO}_2$  NTs diameter and length for biomedical applications. For proteins, not only their size but also the net charge and internal charge distribution affect their binding ability to the negatively charged  $\text{TiO}_2$ . That is protein adhesion on  $\text{TiO}_2$  surface is higher for the positively charged proteins, which is due to the fact that firstly at a physiological pH level the  $\text{TiO}_2$  surface is negatively charged and secondly to more adhesion sites available without encountering hindering steric/charge effects (thus can use to a higher extent the whole length of the nanostructures). Two key aspects of the nanotubular morphology, besides diameter and length, influence protein adhesion and these

are the spacing in between the nanotubes at the top, and the “V-shape” of nanotubes, as adhesion of proteins on the  $\text{TiO}_2$  surface can be hindered (more so for albumin, by other molecules or by the neighboring  $\text{TiO}_2$  surface).

Higher length nanotubes have, as expected, a higher total surface area, and therefore protein adhesion is higher – to account for the influence of the total surface area, dye desorption measurements were used to normalize the active surface area of the investigated nanostructures. Small diameter NTs can bind more small-sized positively charged proteins per surface area, e.g. histone. Theoretical modelling showed that this can be due to the higher density of sharp edges (rims) of the small diameter  $\text{TiO}_2$  nanotubes that leads to an increased magnitude of the surface charge density (negative) at the wall edge and thus to more histone adhesion. This is confirmed by comparing different nanostructures with similar diameter, i.e. NPs and NTs, and although they possess similar surface areas (from dye desorption measurements), there are significant differences in proteins adsorption, NTs adsorb 31% more histone and albumin is detected too. The differences are due to the way the area is distributed: i.e., both inner and outer surface of NTs walls contribute (as there is no significant surface charge density difference between them) compared to the one edge (rim) NPs. This explains why NTs with inner and outer edges, at top, adsorb more histone than the one edge NPs.

Furthermore, protein adhesion on the top surface was evaluated by XPS and ToF-SIMS, revealing higher protein amount on NTs tops for histone compared to albumin and in addition, the protein presence throughout the length was tracked by ToF-SIMS negative sputter depth profiles (via the peptide bonds characteristic to amino acids). The present work points out the importance of  $\text{TiO}_2$  nanostructures' morphology for biomedical applications such as drug delivery or implant materials, where interactions with small size proteins or molecules are primordial.

#### Acknowledgements

The authors acknowledge DFG, Erlangen DFG cluster of excellence and Slovenia Research Agency (ARRS) for financial support. Prof. P. Veranič (Medical Faculty, University of Ljubljana) is acknowledged for the gold labelled antibodies. Dr. S. So is acknowledged for valuable advice regarding the dye desorption measurements. The Ministry of Higher Education, Science and Technology of the Republic of Slovenia within the National Research Program P2-0089, and use of equipment in the Center of Excellence on Nanoscience and Nanotechnology-Nanocenter are acknowledged.

#### Appendix A. Supplementary data

Supplementary data associated with this article can be found, in the online version, at <http://dx.doi.org/10.1016/j.actbio.2016.08.050>.

#### References

- [1] M. Geetha, A.K. Singh, R. Asokamani, A.K. Gogia, Ti based biomaterials, the ultimate choice for orthopaedic implants – a review, *Prog. Mater. Sci.* 54 (2009) 397–425.
- [2] G. Mendonça, D.B. Mendonça, F.J. Aragão, L.F. Cooper, Advancing dental implant surface technology from micron- to nanotopography, *Biomaterials* 29 (2008) 3822–3835.
- [3] S. Bauer, P. Schmuki, K. Von der Mark, J. Park, Engineering biocompatible implant surfaces: part I: materials and surfaces, *Prog. Mater. Sci.* 58 (2013) 261–326.
- [4] A. Shekaran, A.J. Garcia, Nanoscale engineering of extracellular matrix-mimetic bioadhesive surfaces and implants for tissue engineering, *Biochim. Biophys. Acta.* 1810 (2011) 350–360.
- [5] A. Mazare, G. Totea, C. Burnei, P. Schmuki, I. Demetrescu, D. Ionita, Corrosion, antibacterial activity and haemocompatibility of  $\text{TiO}_2$  nanotubes as a function of their annealing temperature, *Corros. Sci.* 103 (2016) 215–222.

- [6] P. Neacsu, A. Mazare, A. Cimpean, J. Park, M. Costache, P. Schmuki, I. Demetrescu, Reduced inflammatory activity of RAW 264.7 macrophages on titania nanotube modified Ti surface, *Inter. J. Biochem. Cell Biol.* 55 (2014) 187–195.
- [7] C. Moerke, P. Mueller, B. Nebe, Attempted caveolae-mediated phagocytosis of surface-fixed micro-pillars by human osteoblasts, *Biomaterials* 76 (2016) 102–114.
- [8] K. Lee, A. Mazare, P. Schmuki, One-dimensional titanium dioxide nanomaterials, nanotubes, *Chem. Rev.* 114 (2014) 9385–9454.
- [9] M. Kulkarni, A. Mazare, E. Gongadze, S. Perutkova, V. Kralj-Iglič, I. Milosev, P. Schmuki, A. Iglič, Titanium nanostructures for biomedical applications, *Nanotechnology* 26 (2015) 062002.
- [10] J. Park, S. Bauer, K. von der Mark, P. Schmuki, Nanosize and vitality: TiO<sub>2</sub> nanotube diameter directs cell fate, *Nano Lett.* 7 (2007) 1686–1691.
- [11] J. Park, S. Bauer, K.A. Schlegel, F.W. Neukam, K. von der Mark, P. Schmuki, TiO<sub>2</sub> nanotube surfaces: 15 nm - an optimal length scale of surface topography for cell adhesion and differentiation, *Small* 5 (2009) 666–671.
- [12] J. Park, S. Bauer, A. Pittrof, M.S. Killian, P. Schmuki, K.V.D. Mark, Synergistic control of mesenchymal stem cell differentiation by nanoscale surface geometry and immobilized growth factors on TiO<sub>2</sub> nanotubes, *Small* 8 (2012) 98–107.
- [13] U. Diebold, The surface science of titanium dioxide, *Surf. Sci. Rep.* 48 (2003) 53–229.
- [14] S. Puckett, E. Taylor, T. Raimondo, T. Webster, The relationship between the nanostructure of titanium surfaces and bacterial attachment, *Biomaterials* 31 (2010) 706–713.
- [15] E. Gongadze, D. Kabaso, S. Bauer, T. Slivnik, P. Schmuki, U. van Rienen, A. Iglič, Adhesion of osteoblasts to a nanorough titanium implant surface, *Int. J. Nanomed.* 6 (2011) 1801–1816.
- [16] M.M. Gentleman, E. Gentlman, The role of surface free energy in osteoblast-biomaterial interaction, *Int. Mater. Rev.* 59 (2014) 418–429.
- [17] C.E. Giacomelli, M.J. Esplandiú, P.I. Ortiz, M.J. Avena, C.P. De Pauli, Ellipsometric study of bovine serum albumin adsorbed onto Ti/TiO<sub>2</sub> electrodes, *J. Colloid Interface Sci.* 218 (1999) 404–411.
- [18] T. Kopac, K. Bozgeyik, J. Yener, Effect of pH and temperature on the adsorption of bovine serum albumin onto titanium dioxide, *Colloids Surf. A Physicochem. Eng. Asp.* 322 (2008) 19–28.
- [19] K. Cai, J. Bossert, K.D. Jandt, Does the nanometre scale topography of titanium influence protein adsorption and cell proliferation?, *Colloids Surf. B* 49 (2006) 136–144.
- [20] C.J. Wilson, R.E. Clegg, D.I. Leavesley, M.J. Percy, Mediation of biomaterial-cell interactions by adsorbed proteins: a review, *J. Tissue Eng.* 11 (2005) 1–18.
- [21] R. Roessler, R. Zimmerman, D. Scharnweber, C. Werner, W. Worch, Characterization of oxide layer on Ti6Al4V and titanium by streaming potential and streaming current measurements, *Colloids Surf. B* 26 (2002) 387–395.
- [22] J. Armstrong, H.J. Salacinski, Q. Mu, A.M. Seifalian, L. Peel, N. Freeman, C.M. Holt, J.R. Lu, Interfacial adsorption of fibrinogen and its inhibition by RGD peptide: a combined physical study, *J. Phys. Condens. Matter* 16 (2004) S2438–S2491.
- [23] M. Kulkarni, Y. Patil-Sen, Ita Junkar, C.V. Kulkarni, M. Lorenzetti, A. Iglič, Wettability studies of topologically distinct titanium surfaces, *Colloids Surf. B* 129 (2015) 47–53.
- [24] W. Peng, Z. Qiao, Q. Zhang, X. Cao, X. Chen, H. Dong, J. Liao, C. Ning, Micropatterned TiO<sub>2</sub> nanotubes: fabrication, characterization and in vitro protein/cell response, *J. Mater. Chem. B* 1 (2013) 3506–3512.
- [25] D. Andelman, Electrostatic properties of membranes: the Poisson-Boltzmann theory, *Handbook of Biological Physics*, Vol. 1, Elsevier Science B.V., 1995.
- [26] M. Kulkarni, A. Flašker, M. Lokar, K. Mrak-Poljšak, A. Mazare, A. Artenjak, S. Cuknik, S. Kralj, A. Velikonja, P. Schmuki, V. Kralj-Iglič, S. Sodin-Semrl, A. Iglič, Binding of plasma proteins to titanium dioxide nanotubes with different diameters, *Inter. J. Nanomed.* 10 (2015) 1359–1373.
- [27] Z.S. Wang, H. Kawauchi, T. Kashima, H. Arakawa, Significant influence of TiO<sub>2</sub> photoelectrode morphology on the energy conversion efficiency of N719 dye-sensitized solar cell, *Coord. Chem. Rev.* 248 (2004) 1381–1389.
- [28] W. Wei, S. Berger, C. Hauser, K. Meyer, M. Yang, P. Schmuki, Transition of TiO<sub>2</sub> nanotubes to nanopores for electrolytes with very low water contents, *Electrochem. Commun.* 12 (2010) 1184–1186.
- [29] M. Kulkarni, A. Mazare, P. Schmuki, A. Iglič, Influence of anodization parameters on morphology of TiO<sub>2</sub> nanostructured surfaces, *Adv. Mater. Lett.* 7 (2016) 23–28.
- [30] H.P. Erickson, N.A. Carrell, Fibronectin in extended and compact conformations, electron microscopy and sedimentation analysis, *J. Biol. Chem.* 258 (1983) 14539–14544.
- [31] E. Gongadze, D. Kabaso, S. Bauer, J. Park, P. Schmuki, A. Iglič, Adhesion of osteoblasts to a vertically aligned TiO<sub>2</sub> nanotube surface, *Mini Rev. Med. Chem.* 13 (2013) 194–200.
- [32] J. Shi, B. Feng, X. Lu, J. Weng, Adsorption of bovine serum albumin onto titanium dioxide nanotube arrays, *Int. J. Mater. Res.* 103 (2012) 889–896.
- [33] G. Arents, R.W. Burlingame, B.-C. Wang, W.E. Love, E.N. Moudrianakis, The nucleosomal core histone octamer at 3.1 Å resolution: a tripartite protein assembly and a left-handed superhelix, *Proc. Natl. Acad. Sci. U.S.A.* 81 (1991) 10148–10152.
- [34] L. Marino-Ramirez, M.G. Kann, B.A. Shoemaker, D. Landsman, Histone structure and nucleosome stability, *Expert Rev. Proteomics* 2 (2005) 719–729.
- [35] J.K. Armstrong, R.B. Wenby, H.J. Meisel, T.C. Fisher, The hydrodynamic radii of macromolecules and their effect on red blood cell aggregation, *Biophys. J.* 87 (2004) 4259–4270.
- [36] H.P. Erickson, Size and shape of protein molecules at the nanometer level determined by sedimentation, gel filtration and electron microscopy, *Biol. Proced. Online* 1 (2009) 32–51, Ed. S. Li.
- [37] D. Burnett, S.M. Wood, A.R. Bradwell, Estimation of the Stokes radii of serum proteins for a study of protein movement from blood to amniotic fluid, *Biochim. Biophys. Acta* 427 (1976) 231–237.
- [38] H.P. Feng, Dale S. Scherl, J. Widom, Lifetime of the histone octamer studied by continuous-flow quasielastic light scattering: test of a model for nucleosome transcription, *Biochemistry* 32 (1993) 7824–7831.
- [39] <http://www.phosphosite.org/proteinAction.action?tid=3634&showAllSites=true>, (last accessed 08.08.16).
- [40] H. Neurath, *The Proteins*, vol. IV, Elsevier, 2012.
- [41] C. Tanford, J.G. Buzzel, The viscosity of aqueous solutions of bovine serum albumin between pH 4.3 and 10.5, *J. Phys. Chem.* 60 (1956) 225–231.
- [42] U. Böhme, U. Scheler, Effective charge of bovine serum albumin determined by electrophoresis NMR, *Chem. Phys. Lett.* 435 (2007) 342–345.
- [43] L.R. Barbosa, M.G. Ortore, F. Spinuzzi, P. Mariani, S. Bernstorff, R. Itri, The importance of protein-protein interactions on the pH-induced conformational changes of bovine serum albumin: a small-angle X-ray scattering study, *Biophys. J.* 98 (2010) 147–157.
- [44] K. Baler, O.A. Martin, M.A. Carignano, G.A. Ameer, J.A. Vila, I. Szleifer, Electrostatic unfolding and interactions of albumin driven by pH changes: a molecular dynamics study, *J. Phys. Chem. B* 118 (2014) 921–930.
- [45] X. Liu, X. Zhou, S. Li, S. Li, R. Lai, Z. Zhou, Y. Zhang, L. Zhou, Effects of titania nanotubes with or without bovine serum albumin loaded on human gingival fibroblasts, *Int. J. Nanomed.* 9 (2014) 1185–1198.
- [46] P. Roy, T. Dey, P. Schmuki, Scanning electron microscopy observation of nanoscopic wetting of TiO<sub>2</sub> nanotubes and ODS modified nanotubes using ionic liquids, *Electrochem. Solid State Lett.* 13 (2010) E11–E13.
- [47] D. Kim, J.M. Macak, F. Schmidt-Stein, P. Schmuki, Capillary effects, wetting behaviour and photo-induced tube filling of TiO<sub>2</sub> nanotube layers, *Nanotechnology* 19 (2008) 305710.
- [48] D.L. Chapman, A contribution to the theory of electrocapillarity, *Philos. Mag.* 25 (1913) 475–481.
- [49] M.G. Gouy, Sur la constitution de la charge électrique à la surface d'un électrolyte, *J. Phys. Radium. J. Physique (France)* 9 (1910) 457–468.
- [50] S. McLaughlin, The electrostatic properties of membranes, *Ann. Rev. Biophys. Chem.* 18 (1989) 113–136.
- [51] D.W.R. Gruen, S. Marčelja, Spatially varying polarization in water, *J. Chem. Soc. Faraday Trans. 79* (1983) 225–242.
- [52] C.W. Outhwaite, Towards a mean electrostatic potential treatment of an ion dipole mixture or a dipolar system next to a plane wall, *Mol. Phys.* 48 (1983) 599–614.
- [53] E. Gongadze, A. Iglič, Decrease of permittivity of an electrolyte solution near a charged surface due to saturation and excluded volume effects, *Bioelectrochemistry* 87 (2012) 199–203.
- [54] M.A. Quiroga, K.H. Xue, T.K. Nguyen, M. Tułodziecki, H. Huang, A.A. Franco, A multiscale model of electrochemical double layers in energy conversion and storage devices, *J. Electrochem. Soc.* 161 (2014) E3302–E3310.
- [55] E. Gongadze, A. Velikonja, Š. Perutkova, P. Kramar, A. Maček-Lebar, V. Kralj-Iglič, A. Iglič, Ions and water molecules in an electrolyte solution in contact with charged and dipolar surfaces, *Electrochim. Acta.* 126 (2014) 42–60.
- [56] S. Puckett, R. Pareta, T.J. Webster, Nano rough micron patterned titanium for directing osteoblast morphology and adhesion, *Int. J. Nanomed.* 3 (2008) 229–241.
- [57] P. Ojeda-May, M.E. Garcia, Electric field-driven disruption of a native β-sheet protein conformation and generation of a helix structure, *Biophys. J.* 99 (2010) 595–599.
- [58] L. Zhao, L. Liu, Z. Wu, Y. Zhang, P.K. Chu, Effects of micropitted/nanotubular titania topographies on bone mesenchymal stem cell osteogenic differentiation, *Biomaterials* 33 (2012) 2629–2641.
- [59] K. Huo, X. Zhang, H. Wang, L. Zhao, X. Liu, P.K. Chu, Osteogenic activity and antibacterial effects on titanium surfaces modified with Zn-incorporated nanotube arrays, *Biomaterials* 34 (2013) 3467–3478.
- [60] M.Y. Lan, C.P. Liu, H.H. Huang, S.W. Lee, Both enhanced biocompatibility and antibacterial activity in Ag-Decorated TiO<sub>2</sub> nanotubes, *PLoS ONE* 8 (2013) e75364.
- [61] S. Ray, A.G. Shard, Quantitative analysis of adsorbed proteins by X-ray photoelectron spectroscopy, *Anal. Chem.* 83 (2011) 8659–8666.
- [62] A. Mazare, I. Paramasivam, F. Schmidt-Stein, K. Lee, I. Demetrescu, P. Schmuki, Flame annealing effects on self-organized TiO<sub>2</sub> nanotubes, *Electrochim. Acta* 66 (2012) 12–21.
- [63] M.S. Killian, P. Schmuki, Influence of bioactive linker molecules on protein adsorption, *Surf. Interface Anal.* 46 (2014) 193–197.
- [64] S. Aoyagi, M. Okamoto, N. Kato, M. Kudo, Analyzing ToF-SIMS spectra of biopolymer using multivariate curve resolution, *J. Surf. Analysis* 17 (2011) 220–223.
- [65] M.S. Wagner, D.G. Castner, Characterization of adsorbed protein films by time-of-flight secondary ion mass spectrometry with principal component analysis, *Langmuir* 17 (2001) 4649–4660.
- [66] Y.S. Hedberg, M.S. Killian, E. Blomberg, S. Virtanen, P. Schmuki, I.O. Wallinder, Interaction of bovine serum albumin and lysozyme with stainless steel studied by time-of-flight secondary ion mass spectrometry and X-ray photoelectron spectroscopy, *Langmuir* 28 (2012) 16306–16317.
- [67] M.S. Killian, H.M. Krebs, P. Schmuki, Protein denaturation detected by time-of-flight secondary ion mass spectrometry, *Langmuir* 27 (2011) 7510–7515.
- [68] N. Mine, B. Douhard, J. Brison, L. Houssiau, Molecular depth-profiling of polycarbonate with low-energy Cs<sup>+</sup> ions, *Rapid Commun. Mass Spectrom.* 21 (2007) 2680–2684.